PROPERTIES OF YOUNG CLUSTERS NEAR REFLECTION NEBULAE

K. Sellgren[1]

California Institute of Technology

ABSTRACT

Near infrared observations in the reflection nebulae NGC 7023, 2023, and 2068 are used to study clusters of young stars found associated with these nebulae. At least 30-60 % of these stars are pre-main sequence objects, as indicated by their infrared excesses, hydrogen line emission, or irregular variability. The spatial distributions and observed luminosity functions of these young open clusters are derived, and the inferred mass function and star formation efficiencies are discussed.

---

1. Observations made partially at the Mt. Wilson Observatory, Carnegie Institution of Washington, as part of a collaborative agreement between Carnegie Institution of Washington and California Institute of Technology.

I. INTRODUCTION

Near infrared observations of dark clouds provide a unique approach to studying low mass star formation. Optical observations are hampered by the large extinctions associated with dark clouds, while radio continuum observations are sensitive only to more massive ionizing stars. Early near infrared searches for embedded stars found an obscured young cluster in the Ophiuchus dark cloud (Grasdalen, Strom, and Strom 1973; Vrba *et al.* 1975), and searches were soon made in many other dark clouds (see Hyland 1981 for a review). Elias (1978*a*,*b*,*c*) showed that many sources found in 2.2 μm scans of dark clouds were background stars not associated with the regions, and that many stars associated with the clouds were pre-main sequence objects. The identification of a substantial background component to 2.2 μm star counts in dark clouds led to an improved understanding of the near infrared extinction in these clouds. The presence of background stars, and of stars not yet on the main sequence, also showed that extreme care must be taken in interpreting near infrared star formation studies in these regions. These effects have been considered in recent estimates of the star formation efficiency in the Chamaeleon dark cloud (Hyland, Jones, and Mitchell 1982).

The observations discussed in this paper are of stars found in the regions near three reflection nebulae, NGC 7023, 2023, and 2068. These stars are shown to be members of young clusters associated with the reflection nebulae. The spatial distributions and luminosity functions of these stars are derived, and estimates of the mass functions and star formation efficiencies are made. The high success rate in finding young clusters of low mass stars is attributable to selecting reflection nebulae for these observations, since this guarantees the absence of high mass (O) stars which would ionize substantial H II regions, while identifying a region of star formation by the presence of a lower mass (B) early

type star still young enough to be physically associated with the cloud from which it formed.

NGC 7023 is at the northern end of a 30' × 60' molecular cloud at a distance of 440 pc (Viotti 1969). The visual reflection nebula is illuminated by the Herbig Be star HD 200775, and the nebula is also associated with a small cluster of T Tauri stars (Weston 1953). NGC 2023 is found in the dark cloud L 1630 (Lynds 1962), and is 20' south of the H II region NGC 2024. The visual reflection nebula is illuminated by the B1.5V star HD 37903. NGC 2068, or M78, is also in L1630. NGC 2068 is 14' south of the active star formation region NGC 2071, and is also 18' north of the Herbig-Haro object HH-24. The visual reflection nebula is illuminated by the northernmost of a pair of stars having $V \sim 10$ mag (Elvius and Hall 1967). These stars, following the notation of Strom *et al.* (1975), will be referred to as HD 38563-N and HD 38563-S. NGC 2023 and 2068 are at a distance of 500 pc (Lee 1968).

The observations reported here include scans at 2.2 μm, and occasionally 1.65 μm, to search for stellar sources; near infrared photometry at 1.25, 1.65, and 2.2 μm for the brighter sources found at 2.2 μm; visual photometry for stars in two of the regions at 0.655 μm; visual and near infrared spectrophotometry for a few stars; and an image tube plate at 0.8 μm of one region. This diverse body of data allows an investigation of the colors, reddening, spectral features, and variability of the stars in these dark clouds. These observations lead to a better understanding of the nature of young stellar objects and low mass star formation occuring in dark clouds, as well as the nature of the dark cloud extinction.

II. OBSERVATIONS

Scans of the reflection nebulae NGC 7023, NGC 2023, and NGC 2068 were made at 2.2 μm, and in some cases, 1.65 μm, using the 100 inch, 60 inch, and 24 inch telescopes at Mt. Wilson Observatory. The areas scanned, wavelength, diaphragm, spacing between source and sky positions, and faintest magnitude detectable are listed in Table 1 for the three nebulae. Adjacent scans were spaced by half the diaphragm diameter. The scans were usually made in nonphotometric conditions, so that the inferred magnitudes are typically reliable to only ~ 0.3 mag, with worse uncertainties in some cases.

A plate of the NGC 7023 region was obtained on the Yerkes Observatory 41 inch reflector, at an effective wavelength of 0.8 μm, using a RG-8 filter and a S-25 image intensifier tube. The 20 brightest stars from this plate were selected and searched for at infrared wavelengths.

Infrared photometry at J (1.25 μm), H (1.65 μm), and K (2.2 μm), using the filters defined by Neugebauer *et al.* (1979), was obtained of many of the stars found in scans and on the 0.8 μm plate. The photometry was calibrated relative to the standard stars given by Elias *et al.* (1982).

Photometry at a wavelength of 0.655 μm, using an r filter as defined by Thuan and Gunn (1976), was obtained for stars in NGC 2023 and NGC 2068 on 1981 September 25. This photometry was derived from 11 direct SIT frames taken on the Palomar 60 inch telescope, using standard techniques described by Kent (1979). Nonphotometric sky conditions resulted in photometric uncertainties of ± 0.2 mag.

A spectrum with a resolution of $\Delta\lambda/\lambda = 1.7 \times 10^{-3}$, from 2.15 to 2.22 μm, was obtained of HD 200775 on 1980 October 9 with the Mt. Wilson Observatory 60 inch telescope. This spectrum was measured with a Fabry-Perot spectrometer, using techniques described in more detail by Sellgren *et al.* (1983*a*).

Spectra from 0.38 μm to 0.76 μm were obtained of 3 stars in NGC 2023 and NGC 2068 on 1981 August 30-31, using the Palomar 200 inch telescope and the double spectrograph blue camera described by Oke and Gunn (1982).

III. RESULTS

a. *Photometry*

The observations of stars in NGC 7023, 2023, and 2068 are presented in Table 2. The designation given in the first column will be the notation used to refer to the stars throughout this paper, although other designations are also given in Table 2 when available.

Table 2 contains 30, 14, and 56 stars found in NGC 7023, 2023, and 2068 respectively at infrared wavelengths, as well as some stars found only at visual wavelengths. Of these stars, respectively 11, 8, and 15 are brighter than K = 10.5 mag in scan areas typically 6-8' on a side.

The background star count model of Jones *et al.* (1981) can be used to estimate the expected number of background stars in these scan areas. This model agrees very well with observations of background stars in many regions. In particular scans of a 2.4 square degree region near NGC 7023 (Elias 1983, private communication) find 19.2 ± 2.8 stars per square degree brighter than K = 7.5 mag, while the model predicts 15.4 stars per square degree brighter than K = 7.5 mag, in good agreement with the observations. The background star count model predicts that at the galactic latitudes of NGC 7023, 2023, and 2068, 14.2°, 16.6°, and 14.5°, one expects 120, 75, and 86 background stars per square degree with $K \leq 10$ mag, respectively. Similarly one expects 230, 150, and 170 background stars per square degree, respectively, with $K \leq 11$ mag. Thus in the areas scanned only 2 or less background stars with $K \leq 10.5$ mag are expected. Many more stars than this were found in each nebula, so that 75–90% of the stars found in near infrared scans are stars physically associated with the reflection nebulae. This confirms the suggestions of other observers of NGC 7023 (Weston 1953; Strom *et al.* 1972), NGC 2023 (Strom *et al.* 1975), and NGC 2068 (Herbig and Kuhi 1963; Strom *et al.* 1975; Strom, Strom and Vrba 1976) that

these regions contain clusters of young stars. Further arguments for a large fraction of stars physically associated with the clouds are the clear spatial clustering of the stars and the identification of many stars as pre-main sequence stars, as discussed in more detail in sections IVb and IVc.

Photometry at J, H, and K was obtained for some of these stars, and is given in Table 2. All J, H, and K photometry for each star was obtained on the same night, so that possible variability of a star should not affect its infrared colors. The $J-H$ and $H-K$ stellar colors are plotted in Fig. 1 for each nebula. In these $J-H$ *vs.* $H-K$ diagrams, the reddening line (cf. section IVa) is drawn through a point corresponding to the average color of a foreground or background star, which model predictions at 2.2 μm indicate is most likely a K giant. The reddening line for an early type main sequence star is also shown.

In NGC 7023 (Fig. 1a) most of the stars appear to have colors appropriate to a normal reddened star. Three stars, however, fall substantially below the reddening line for early type stars, implying that these stars have an infrared excess. The remaining stars are, by their colors, consistent with either being background giants or stars without strong infrared excesses associated with the cloud. In NGC 2023 (Fig. 1b), almost half the stars observed fall below the reddening line for early type stars, and therefore have infrared excesses. The color-color diagram for NGC 2068 is shown in Fig. 1c. Of the stars in NGC 2068 whose photometry is reported in Table 2, stars 5, 15, 19, and 30 have infrared excesses. For NGC 2068 the photometry of this paper was supplemented by the observations of Strom, Strom, and Vrba (1976), transformed to the photometric system of Neugebauer *et al.* (1979) using the relation of Frogel *et al.* (1978). Of the stars listed in Table 2 for which the colors of Strom *et al.* have been adopted, stars 4 and 2 have infrared excesses, while stars 20 and 53 have no evidence for infrared excesses. All stars in the three nebulae with identified

infrared excesses have this noted in Table 2.

The r photometry in NGC 2023 and 2068 is also presented in Table 2. Typically $r-K \sim 6$ mag in the two nebulae. The stars detected at only r or K, but not both, have upper or lower limits on $r-K$ generally consistent with $r-K \sim 6$ mag also.

b. Spectrophotometry

A spectrum of HD 200775 was obtained from 2.15 to 2.22 μm with $\Delta\lambda/\lambda = 1.7 \times 10^{-3}$. B γ was seen in emission from the star, with a strength of 2.3×10^{-12} erg cm^{-2} s^{-1}, and was unresolved with an instrumental resolution of 500 km s^{-1}. A 3 σ upper limit of 9×10^{-13} erg cm^{-2} s^{-1} was placed on other possible features in the spectrum.

Visual spectrophotometry was obtained for two stars in NGC 2023, stars H and C, and for one star in NGC 2068, star 20. The continua of these stars are extremely red, with $B-V$ = 1.6, 1.8, and 2.2 mag respectively for 2023-H, 2023-C, and 2068-20. In 2023-H and 2023-C, H α is seen in emission from the star, while in 2068-20 both H α and H β are seen in emission. H α emission was previously identified in 2068-20 by Herbig and Kuhi (1963), who refer to this star as LkHα 304.

The hydrogen line emission in HD 200775, 2023-H, 2023-C, and 2068-20 must come from dense circumstellar shells or stellar winds. This is because the observed B γ and H α fluxes would predict optically thin free-free emission at radio wavelengths, far in excess of the 6 cm upper limits observed by Sellgren *et al.* (1983b) for these stars.

c. Variability

The observations reported here also include measurements at K, and sometimes H, made at different times, which can be used to investigate the variability of the stars observed in the three reflection nebulae. Both scan

magnitudes and photometric magnitudes obtained on different dates are presented in Table 3, as well as measurements by other observers when available. Only stars suspected of variability are included in this table.

In comparisons between different sets of photometry, with uncertainties ~ 0.05 mag, differences ≥ 0.15 mag were considered evidence of variability. When comparisons included scan magnitudes, which are uncertain by ≳ 0.3 mag, differences ≥ 0.75 mag were taken as evidence of variability. Only differences ≥ 0.75 mag were considered in establishing variability based on comparisons between the measurements presented in this paper and those of other observers, due to the possibility of unknown systematic differences between the various sets of data.

In NGC 7023, 6 stars are definitely identified as variable stars, based on photometry, while another 3 stars may be variable, based on scan magnitudes. Only the stars whose photometric magnitudes varied are identified as variable in Table 2a. These 6 stars varied by amounts ranging from 0.17 mag to 0.59 mag at K. The shortest time scale variability was seen in star D, where two photometric measurements on 1981 July 28, separated by 5 hours, differed by 0.15 ± 0.04 mag at *K*. HD 200775 (star A) was extensively observed at *J*, *H*, and *K*. Although this star is a Herbig Be star, stars which as a class are frequently variable, HD 200775 itself shows no evidence for infrared variability on time scales of hours, days, or years.

There is little evidence of variability ≥ 0.75 mag for the stars in NGC 2023. Star F appeared to vary by 1.4 mag at *K* from intercomparisons of different scans and photometry, but this is probably due to confusion (see footnote to Table 2b).

In NGC 2068 13 stars may have varied by ≥ 0.75 mag. Evidence for variability in stars 13 and 15 depends on single bright *K* measurements on the

Mt. Wilson 24 inch telescope, near the scan detection limit. The variation in stars 26a and 26b is likely due to confusion. The remaining 9 stars have been identified as variable in Table 2*a*. Star 14 varied 0.9 mag at *H*, based on measurements of other observers (Strom *et al.* 1975; Strom, Strom, and Vrba 1976). The other 8 stars varied by amounts ranging from 1.0 mag to 1.5 mag at *K*.

It is important to realize that while the fractions of stars found to vary in NGC 2023 and 2068 are less than in NGC 7023, the variability identified in NGC 7023 would have been missed if two sets of photometry separated by two years had not been available. Only one set of photometry exists in the other two nebulae, so that only variability ≥ 0.75 mag can be detected by comparison with scan magnitudes. The largest variation in the NGC 7023 photometry is smaller than this. This suggests that additional photometry in NGC 2023 and 2068 may uncover many more variable stars.

IV. DISCUSSION

a. Near infrared extinction in reflection nebulae

The reddening line in Fig. 1, $E(J-H)/E(H-K) = 1.90$, is derived from the value of Jones and Hyland (1980), measured on the AAO photometric system, by transforming it (Elias *et al.* 1983) to the photometric filters used here. A slightly different value, $E(J-H)/E(H-K) = 1.6$, has been obtained by Elias (1978c). Use of this reddening law instead would have no effect on the numbers of pre-main sequence stars found or on other conclusions of this paper.

Jones and Hyland (1980) have argued that the extinction curve in the near infrared, at least at J, H, K, and perhaps L (3.4 μm), is identical, within the uncertainties, in the general interstellar medium and in dense molecular clouds where large values of $R = A_V/E(B-V)$ have been reported. As discussed by Hyland (1981), the upper envelope of a $J-H$ *vs.* $H-K$ diagram for the stars observed towards a dark cloud is composed of background late type giants and stars without infrared excesses associated with the cloud, and therefore defines the near infrared extinction curve in the dark cloud. As can be seen from the good agreement between the reddening line of Jones and Hyland (1980) indicated in Fig. 1 and the observed upper envelopes to the color-color diagrams, the observed near infrared extinction curves in these three reflection nebulae support the hypothesis that a single near infrared extinction curve applies in a wide variety of physical environments.

While the near infrared extinction curve, as defined by $E(J-H)/E(H-K)$, is seen to be constant, the absolute value of the extinction is not known. Jones and Hyland (1980) fit a power law to their infrared extinction curve at J, H, K, and L, and find that at these wavelengths that the extinction is consistent with a $\lambda^{-2.5}$ power law. This neglects the possibility of a grey component to the near

infrared extinction. Without more information on the absolute value of the near infrared extinction, it seems reasonable to adopt an extinction proportional to $\lambda^{-1.5}$, which implies that $E(J-H)/A_K = 2.06$ and $E(H-K)/A_K = 1.05$. These values are adopted throughout this paper.

b. The fraction of stars which are pre-main sequence

To determine the fraction of the total number of stars which are pre-main sequence (PMS), one must first restrict the sample so that it is complete and reasonably uniform. For this reason the only stars considered are those found in 2.2 μm scans in 1979 of NGC 7023, with a detection limit of 11.0 mag; 2.2 μm scans in 1981 January of NGC 2023, with a detection limit of 11.1 mag; and 2.2 μm scans in 1981 September and 1981 November of NGC 2068, with detection limits of 11.9 - 12.6 mag. These samples are estimated to be complete to K = 10.5 mag for NGC 7023 and 2023, and to 11.25 mag for NGC 2068. Stars below the scan completeness limit in each case are excluded from the sample. This provides uniform selections of stars in each nebula found from a set of scans with a single completeness limit, over a wide area. The small fraction of background stars, 10 - 25%, will be neglected in determining the characteristics of the stellar clusters associated with the reflection nebulae. The scan areas for these samples are 0.58, 1.39, and 1.26 pc^2 respectively for NGC 7023, 2023, and 2068. The stars included in the sample are all stars in Table 2 brighter than the scan completeness limit, except for stars 40 and 42 in NGC 7023, stars L and N in NGC 2023, and stars 1, 2, 3, 4, 5, 6, and 55 in NGC 2068. Note that star D in NGC 7023 is included in the sample, since it was brighter than the scan completeness limit when first discovered (Table 3a).

Some of the stars which are listed in Table 2a are also identified with variable or suspected variable stars found by Rosino and Romano (1962). When suitable observations exist at both wavelengths, all of the stars known to vary in

NGC 7023 are seen to be variable at both visual and near infrared wavelengths. The study of Rosino and Romano (1962), which is more extensive in its time coverage, shows that the stars in NGC 7023 vary irregularly with time, which is characteristic of nebular variables such as T Tauri stars. The time coverage of the observations reported in Table 3 is not complete enough to establish the nature of the variability of the stars observed in the three reflection nebulae. The good correspondence between variability at K and identification as an irregular variable at visual wavelengths in NGC 7023, however, suggests that it is a reasonable assumption that infrared variability indicates that a star is a PMS star physically associated with the cloud.

The variety of observations described above provide an approach to estimating the number of young PMS stars in the reflection nebula fields. One method of identifying a PMS star is by its variability. The presence of an infrared excess or Hα emission, both of which are indicators of circumstellar shells which surround PMS stars (Strom, Strom, and Grasdalen 1975), can also be used to identify PMS stars. These three characteristics are noted in Table 2 for each star that is known to show them.

In the sample which has been restricted so as to be complete, 6 out of 11 stars in NGC 7023 are identified as PMS stars, using the criteria of variability, infrared excesses, and hydrogen line emission. Similarly 5 out of 8 stars in NGC 2023, and 9 out of 26 stars in NGC 2068, are PMS stars. Many of the irregular variables in NGC 7023 show no evidence of an infrared excess in the color-color diagrams, but the observations of this paper are not sufficient to determine the variability of most stars in NGC 2023 and 2068. Thus these numbers set lower limits to the fraction of the detected stars which are PMS stars.

All the stars in NGC 2023 and 2068 cannot be PMS, since star A in NGC 2023 is classified B1.5V (Abt and Levato 1977), and stars 31 and 36 in NGC 2068 are

classified ~ B3V (Sellgren *et al.* 1983b). These stars, in addition to star 33 in NGC 2068 (B2II-III; Strom *et al.* 1975) appear to be normal stars with no evidence of variability, H α emission, or infrared excesses. The earliest type star in NGC 7023, HD 200775, is a PMS star (Strom *et al.* 1972), with an infrared excess and H α emission, although it is not photometrically variable (section IIIc; Breger 1974). The remaining stars in NGC 7023 are either PMS or unclassified, so it is possible that no stars in NGC 7023 have reached the main sequence yet.

c. The luminosity function and spatial distribution of the stars

The spatial distibution of stars in the three nebulae is shown in Fig 2. The surface density of stars can be seen to be highest near the cluster centers, which in NGC 2068 and NGC 7023 is consistent with the positions of the visual illuminating stars of the reflection nebulae, star 33 and star A respectively. In NGC 2023 the visual illuminating star, star A, does not appear to be at the center of the cluster, so the NGC 2023 cluster center is assumed to be the mean position of the stars, 60" east and 67" south of star A. The radial distribution of stars from the cluster center for each nebula appears to follow a power law of the form $N(R) \sim R^x$, where $N(R)$ is the total number of stars inside of a circle of projected radius R. Power laws were found for NGC 7023, 2023, and 2068 of $x = 0.94 \pm 0.28$, $x = 0.83 \pm 0.33$, and $x = 0.89 \pm 0.10$, respectively, using only the stars in the samples which have been limited so as to be complete. These are all consistent with $x = 1$, or $N(R) \sim R$. This distribution corresponds to a surface density of stars $\sigma(R) \sim R^{-1}$, if σ is uniform. If the clusters are spherically symmetric, the observed distribution $N(R)$ also corresponds to a volume density of stars $n(r) \sim r^{-x}$, where r is the true radius from the cluster center.

The distribution in apparent magnitude can also be determined from the observations of the three reflection nebulae. The cumulative number of stars

$N(K)$ *vs.* observed K magnitude is shown in Fig. 3 for NGC 2068, where the largest number of stars were found. This figure includes data from all the K scans, up to a K magnitude 0.5 mag brighter than each scan detection limit, scaled to account for the different surface densities of stars sampled by different scans, and weighted by the uncertainties due to counting statistics in each magnitude bin. The assumption is made that $N(K)$ is independent of position in the nebula. The observed distribution suggests a form for the observed luminosity function of $N(K) \sim 10^{\gamma K}$. In NGC 2068 the observed value of γ is $\gamma = 0.29 \pm 0.03$. In NGC 7023 and NGC 2023, the number of stars is smaller and the uncertainties therefore larger, but consistent results are found of $\gamma = 0.24 \pm 0.05$ and $\gamma = 0.21 \pm 0.09$ respectively.

The relationship between the observed luminosity function, $N(K)$, and the intrinsic luminosity function $n(K_0)$, where K_0 is the absolute K magnitude, and $n(K_0)$ is the number of stars in a magnitude interval dK_0, depends on a number of characteristics of the cluster, such as the spatial distribution of stars and dust. However, as long as $n(K_0)$ is everywhere the same in the nebula, then for $N(K) \sim 10^{\gamma K}$, as was found for the three reflection nebulae, $n(K_0) \sim 10^{\gamma K_0}$. This also assumes that any cutoff or change in slope in $n(K_0)$ does not occur within the observed magnitude range of the sample from which $N(K)$ was derived. For the finite number of stars observed here, it is possible that differences in the reddening of individual stars will alter the slope of the observed luminosity function. Since the reddening deduced from the color-color diagrams (Fig. 1), however, is typically only $A_K \sim 0.5$ mag, and at most $A_K \sim 1$ mag, while the observed luminosity function is determined over 4 magnitudes at K, the reddening of individual stars should have little effect on the slope of the intrinsic luminosity function derived from the observations.

To convert the observed luminosity function $n(K_0)$ into a mass function one needs to know the relation between absolute K magnitude and stellar mass. This relation is completely unknown for the PMS stars, which comprise at least 30% of the stars in NGC 2068. A simple-minded approach is to assume the mass-luminosity relation for PMS stars has the same slope as the main sequence mass-luminosity relation. This assumption is more or less equivalent to assuming that the ratio of PMS to main sequence stellar luminosity is approximately independent of spectral type within a given cluster. This simplistic assumption appears to be a fair approximation to published 2.2 μm observations of PMS stars in other regions, for a wide range in spectral types, and to the H-R diagrams derived by Cohen and Kuhi (1979) for PMS stars, which show the PMS stars in a cluster to generally lie in a band on the H-R diagram parallel to and above the main sequence.

A second problem in estimating the mass function is that the observed luminosity function contains contributions from both PMS and main sequence stars. For this the simplifying assumption is made that the fraction of PMS stars is the same at each observed luminosity. While an increasing fraction of PMS stars with decreasing luminosity might be expected to be more appropriate, a constant fraction is consistent with the observations and more complicated expressions do not seem warranted.

With these two simple-minded assumptions, then, the main sequence mass-luminosity relation combined with the derived cluster luminosity function can be used to estimate the cluster mass function. The main sequence mass-luminosity relation, for main sequence stars, is approximately $L_K \propto M^{2.4}$, where L_K is the luminosity at 2.2 μm and M is the mass. Since $L_K \propto 10^{-0.4K_0}$, the luminosity function $n(K_0) \sim 10^{\gamma K_0}$ implies a power law distribution with mass, $n(M) \sim M^{\beta}$, where β is the power law index for mass, and $n(M)$ is the number of

stars in a logarithmic mass interval $d\log M$. From the observed luminosity function in NGC 2068, with the above assumptions, one derives a mass power law index of $\beta = -1.8 \pm 0.2$. This is not significantly different from the standard Salpeter mass power law index $\beta = -1.35$, and agrees well with the range of mass power law indices observed in associations of T Tauri stars, $\beta = -1.35$ to -2.9 (Cohen and Kuhi 1979).

d. The stellar density and star formation efficiency

Norman and Silk (1980) have described a scenario for star formation in dark clouds where stellar winds from T Tauri stars in the clouds provide the energy input for further formation of T Tauri stars. This theory explains the noncoeval star formation in dark clouds suggested by the observed spread of ages of T Tauri stars in the same cloud. Norman and Silk argue that densities of T Tauri stars above a critical density of 10 pc^{-3} are needed for this mechanism to work, and so it is of interest to calculate the density of T Tauri stars in NGC 7023, 2023, and 2068.

The spatial densities of the stars in NGC 7023, 2023, and 2068 can be estimated in two ways. First, one can assume spherical symmetry. Second, one can estimate the extent of the cloud along the line of sight by a comparison of the gas density n_H and the gas column density N_H, and then assume that the stars and gas are coextensive. The gas density and gas column density can be obtained from molecular line observations.

For NGC 7023, the column density of ^{13}CO is 1×10^{16} cm^{-2} (Loren, VandenBout, and Davis 1973), and the hydrogen density is $\sim 10^3$ cm^{-3} (Whitcomb *et al.* 1981). For a ^{13}CO to hydrogen ratio of 2×10^{-6} (Dickman 1975), the approximate line of sight distance is ~ 2 pc. For NGC 2023, the column density of ^{13}CO is 1×10^{17} cm^{-2} (Milman *et al.* 1975), and the hydrogen density implied by the C II observations (Pankonin and Walmsley 1978) is $\sim 5 \times 10^4$ cm^{-3}, so that

the line of sight distance is ~ 0.4 pc. For NGC 2068 the column density of ^{13}CO is 6×10^{16} cm^{-2} (Milman *et al.* 1975), and the hydrogen density is 4×10^{4} cm^{-3} (Loren 1981), implying a line of sight distance of ~ 0.2 pc. The scan areas in NGC 7023, 2023, and 2068, for the sample which has been limited so as to be complete, are respectively 0.58, 1.4, and 1.3 pc^{2}, and contain 6, 5, and 9 known PMS stars. Assuming spherical symmetry, the number densities of PMS stars are ~ 10, 3, and 6 pc^{-3} in NGC 7023, 2023, and 2068. Adopting instead the line of sight distances from a comparison of N_H and n_H gives PMS stellar densities of ~ 6, 10, and 30 pc^{-3}, respectively. The actual densities of PMS stars are likely higher, since there are probably PMS stars fainter than the scan limits, and also the methods of this paper for identifying PMS stars provide only lower limits to their numbers. Thus, the densities of PMS stars in these three regions are comparable to the densities required by the model of Norman and Silk (1980) to maintain continuing low mass star formations in dark clouds.

A comparison of the column densities of stars and gas does not depend on uncertain estimates of the line of sight extent of the stellar cluster. An effective star formation efficiency is then the ratio of the mass per unit area in stars to the combined mass per unit area of stars plus gas. The most conservative estimate is to assume all stars whose spectral types are unknown are PMS stars, since these stars are less massive than a main sequence star of the same luminosity; to make no correction for possible reddening of the stars; and to include only stars already found in the scans limited so as to be complete. This estimate will therefore be a strong lower limit, especially since there are presumable fainter stars which contribute considerably to the mass of the cluster. The estimates of stellar mass contained in the areas scanned in NGC 7023, 2023, and 2068 are respectively 10, 10, and 30 $M_{\odot}$ under these assumptions. The masses are ~ 10-40% higher if stars in Table 2 below the scan

completeness limits are included. The gas mass per unit area is found from the ^{13}CO column densities above. The observed lower limits to the effective star formation efficiencies in NGC 7023, 2023, and 2068 are ~ 30%, 2%, and 10% respectively. These efficiencies would be ~ 50%, 3%, and 20% if stars not known to be PMS stars were assumed to lie on the main sequence. While the conversion of gas into stars in NGC 7023 appears to be relatively efficient, this reflects in part the fact that the NGC 7023 stellar cluster is not at a molecular peak. In all three nebulae the molecular gas extends over a larger area than does the stellar cluster, so that the total star formation efficiency for the cloud is much lower than the local efficiency within the cluster. It would be extremely interesting to examine how the efficiency of star formation varied with radius in the stellar cluster. This comparison, however, must await molecular line observations with higher resolution than the angular resolution of ~ 3' presently available.

V. SUMMARY

The properties of stars found in 2.2 μm scans of reflection nebulae have been investigated, and several conclusions about the nature of the stars can be drawn:

1. The number of stars found is much larger than the number of expected background stars, implying that almost all of the stars found are in fact associated with the cloud.

2. Consideration of a number of indicators of the pre-main sequence (PMS) nature of stars, such as hydrogen line emission, infrared excesses, or irregular variability, shows that at least 30-60 % of the stars found in these stellar clusters have not reached the main sequence.

3. The observed variability indicates that at least 50 % of the stars in NGC 7023 are PMS objects, but most of the nebular variable stars in NGC 7023 do not have identifiable infrared excesses. This suggests that identification of young stars by their infrared excesses, as was done in NGC 2023 and 2068, severely underestimates the true numbers of PMS stars.

4. The observed luminosity function of the young stellar clusters is found to be $N(K) \sim 10^{\gamma K}$, with $\gamma = 0.29 \pm 0.03$.

5. The star formation efficiency local to the stellar cluster is found to be at least 30 % in NGC 7023, although the overall efficiency for the entire dark cloud is lower.

6. The spatial densities of PMS stars are found to be $\gtrsim$ 3-30 pc^{-3}, comparable to values required by the model of Norman and Silk (1980) to maintain constant low mass star formation in the dark clouds.

7. The surface density of the stars in all three nebulae decreases as the inverse of the projected radius from the cluster center. This, if spherically symmetric, corresponds to a volume density which depends on the true radius as r^{-2}.

Acknowledgements

I thank the staff of Mt. Wilson Observatory for their hospitality, and my night assistants M. Deak, J. Frazer, and H. Lanning. Additional assistance with the observations was provided by M. Ashley, G. Berriman, E. Grossman, J.H. Lacy, M. Malkan, P. McGregor, J.E. Nordholt, A.J. Rosenthal, B.T. Soifer, S.E. Whitcomb, and R.L. White. I especially thank S.E. Whitcomb, who contributed significantly to the initial observations of stars in NGC 7023. I thank M.W. Werner and A. Bentley for obtaining photometry of HD 200775 for me; S. E. Whitcomb for obtaining a 0.8 μm photograph of NGC 7023; J.G. Cohen for obtaining visual spectra of 3 stars in NGC 2023 and 2068; M. Malkan for obtaining SIT frames in NGC 2023 and 2068 and helping with their reduction; T. Jones for providing model predictions of background star counts; Yerkes Observatory and the University of Wyoming for the use of their telescope facilities; G. Grasdalen for a careful reading of the manuscript; and J. Elias for communication of unpublished data. Useful discussions were held with J.G. Cohen, S.E. Whitcomb, J. Elias, B.T. Soifer, and G. Neugebauer. This research was supported by grants from NASA and NSF.

REFERENCES

Abt, H.A. and Levato, H. (1977). Pub. Astron. Soc. Pac. **89**, 797.

Breger, M. (1974). Astrophys. J. **188**, 53.

Cohen, M. and Kuhi, L. V. (1979). Astrophys. J. Suppl. **41**, 743.

Dickman, R.L. (1975). Ph.D. thesis, Columbia University.

Elias, J.H. (1978a). Astrophys. J. **223**, 859.

Elias, J.H. (1978b). Astrophys. J. **224**, 453.

Elias, J.H. (1978c). Astrophys. J. **224**, 857.

Elias, J.H., Frogel, J.A., Matthews, K., and Neugebauer, G. (1982). Astron. J. **87**, 1029.

Elias, J. H., Frogel, J. A., Hyland, A. R., and Jones, T. J. (1983). Submitted to Astron. J.

Elvius, A. and Hall, J.S. (1967). *Interstellar Grains*, eds. J.M. Greenberg and T.P. Roark

Frogel, J.A., Persson, S.E., Aaronson, M., and Matthews, K. (1978). Astrophys. J. **220**, 75.

Grasdalen, G.L., Strom, K.M., and Strom, S.E. (1973). Astrophys. J. Lett. **184**, 53.

Herbig, G.H. and Kuhi, L.V. (1963). Astrophys. J. **137**, 398.

Herbig, G.H. and Rao, N.K. (1972). Astrophys. J. **174**, 401.

Hyland, A.R. 1981, in IAU Symposium **96**, *Infrared Astronomy*, eds. C.G. Wynn-Williams and D.P. Cruikshank (Reidel, Dordrecht).

Hyland, A. R., Jones, T. J., and Mitchell, R. M. (1982). Mon. Not. R. Astron. Soc. **201**, 1095.

Jones, T.J., and Hyland, A.R. (1980). Mon. Not. R. Astron. Soc. **192**, 359.

Jones, T.J., Ashley, M., Hyland, A.R., and Ruelas-Mayorga, A. (1981). Mon. Not. R. Astron. Soc. **197**, 413.

Kent, S.M. (1979). Pub. Astron. Soc. Pac. **91**, 394.

Lee, T.A. (1968). Astrophys. J. **152**, 913.

Loren, R.B., VandenBout, P.A., and Davis, J.H. (1973). Astrophys. J. Lett. **135**, 67.

Loren, R. B. (1981). Astron. J. **86**, 69.

Lynds, B. T. (1962). Astrophys. J. Suppl. **7**, 1.

Milman, A.S., Knapp, G.R., Kerr, F.J., Knapp, S.L., and Wilson, W.J. (1975). Astron. J. **80**, 93.

Neugebauer, G., Oke, J.B., Becklin, E.E., and Matthews, K. (1979). Astrophys. J. **230**, 79.

Norman, C., and Silk, J. (1980). Astrophys. J. **238**, 158.

Oke, J.B., and Gunn, J.E. (1982). Pub. Astron. Soc. Pac. **94**, 586..

Pankonin, V. and Walmsley, C.M. (1978). Astron. Astrophys. **67**, 129.

Romano, G. (1975). Astrophys. Space Sci. **33**, 487.

Rosino, L., and G. Romano (1962). Contr. Asiago Obs. *127*.

Sellgren, K., Soifer, B.T., Neugebauer, G. and Matthews, K. (1983a). Pub. Astron. Soc. Pac., to be published.

Sellgren, K., Becker, R., Pravdo, S.H., and White, R.L. (1983b). In preparation.

Strom, K.M., Strom, S.E., Carrasco, L., and Vrba, F.J. (1975). Astrophys. J. 198, 489.

Strom, K.M., Strom, S.E., and Vrba, F.J. (1976). Astron. J. 81, 308.

Strom, S.E., Strom, K.M., Yost, J., Carrasco, L., and Grasdalen, G. (1972). Astrophys. J. 173, 353.

Strom, S.E., Strom, K.M., and Grasdalen, G.L. (1975). Ann. Rev. Astron. Astrophys. 13, 187.

Thuan, T.X., and Gunn, J.E. (1976). Pub. Astron. Soc. Pac. 88, 543.

Viotti, R. (1969). Mem. Soc. Astr. Ital. 40, 75.

Vrba, F.J., Strom, K.M., Strom, S.E., and Grasdalen, G.L. (1975). Astrophys. J. 197, 77.

Weston, E.B. (1953). Astron. J. 58, 48.

Whitcomb, S.E., Gatley, I., Hildebrand, R.H., Keene, J., Sellgren, K., and Werner, M.W. (1981). Astrophys. J. 246, 416.

Table 1

λ (μm)	scan limits α[a]	δ[a]	$m_{1\mu m}$[b]	date	θ[c] (")	spacing[d] (")	scan direction[e]
			a. Scans of NGC 7023				
1.65	23E-23W	23S-158S	11.3	1979AUG22	11	20	ra
	23E-23W	23N-203N					
2.2	158E-113W	203N-203S	11.0	1979AUG23-24	11	20	ra
	113W-158W	23N-113S					
2.2	113W-158W	23N-203N	11.0	1979SEP03	11	32	ra
	113W-158W	113S-203S					
	23E-68E	23S-68N					
2.2	158E-203E	203S-203N	11.7	1981JUL30-AUG01	11	23	ra
	203W-158W	203S-113N					
	203E-316E	68S-23N					
	203W-312W	68S-23N					
2.2	129E-424E	15N-176N	12.0	1981NOV15-21	16	129	dec
	462W-301W	157S-4N					
	81W-81E	81S-81N					
	148E-172E	214S-52S					
			b. Scans of NGC 2023				
2.2	250E-250W	273N-200S	11.1	1981JAN05-08	20	70	dec
2.2	50W-50E	100S-100N	11.1	1981JAN07	10	70	dec
2.2	136E-310E	23S-68N	11.0	1981FEB01	11	36	ra
	226W-307W	23S-68N					
2.2	*f*	*f*	*f*	1981OCT20	19	344	ra
			c. Scans of NGC 2068				
1.65	0W-382W	382S-67N	11.0	1981FEB03-05	19	344	ra
2.2	0W-382W	29N-191N	10.6	1981FEB06-12	19	344	ra
	382W-764W	48S-191N					
2.2	50E-50W	0N-100N	12.6	1981SEP16-17	10	60	dec
2.2	50E-250E	0N-100N	11.9	1981SEP17-19	20	60	dec
2.2	0W-382W	0S-161S	8.7	1981OCT13-14	19	344	ra
2.2	90E-0E	100S-200S	11.9	1981NOV11	20	55	dec
2.2	161E-161W	0S-322S	12.0	1981NOV17-20	16	129	dec
	0W-322W	161N-0N					
	322E-161E	0S-161S					
	161E-81E	205N-44N					

(a) Offset in arcsec from HD 200775 = star A in NGC 7023, from HD 37903 = star A in NGC 2023, and from HD 38563-N = star 33 in NGC 2068.

(b) Faintest magnitude detectable

(c) Diameter of diaphragm

(d) Spacing between source and sky positions

(e) The scan technique used was a raster scan covering the area indicated. The direction of the scan lines was along the line connecting the source and sky positions.

(f) Specific search for a particular star rather than a systematic scan.

Table 2a

Stars found in 2.2 and 1.65 μm scans of NGC 7023

name	K[a]	H[a]	J[a]	σ(K)[b]	σ(H)[b]	σ(J)[b]	Δα[c]	Δδ[c]	Δpos[d]	Other designations[e]	PMS[f]
42	10.1						472W	191S	5		
41	10.7						442W	73S	5		
40	7.7						416W	77S	5		
39	12.0						349W	6S	5		
38	11.05	11.51	12.21			0.06	220W	6S	5	S3	
F	10.74	10.94	11.49			0.06	156W	140S	3		
I	10.35	10.74	11.72			0.09	136W	34N	3	S4	
J	8.97	9.62	10.67			0.07	59W	52N	3	R2, S5, *g*	I,V
K	9.38	9.80	10.64	0.06		0.09	34W	49N	3		
E	10.88	11.30	12.22			0.10	5W	88S	3	S3, S2, LkHa 425	H,V
A	4.62	5.42	6.09				0E	0N	3	HD 200775, MWC 361, BD +67° 1283	H,I
L	9.30	9.64	10.49				7E	106N	3	SX Cep	V
M	11.01	11.37	12.13			0.07	25E	75N	3	S6	
N	10.29	10.76	11.65	0.06		0.11	35E	192N	3	R5, S8	V
D	10.53	10.88	11.38			0.06	38E	11S	3	RS3, HZ Cep	V
B	9.61	9.77	10.42			0.06	46E	183S	3		
C	10.25	10.84	11.64			0.09	64E	64S	3	R6, S1, FU Cep, LkHa 427, A	H,I,V
29	11.7						77E	23S	5		
44	11.5						89E	0N	5		
10	11.7						99E	128S	3		
S	12.44	12.72	14.37	0.11	0.06	0.27	127E	50S	3		
O	10.40	10.86	11.74			0.07	135E	109N	3	S11	
45	12.0						148E	194S	5		
T	11.23	11.47	12.36			0.07	173E	32S	3		
46	10.9						177E	227S	5		
34	11.2						192E	150S	3		
30	9.47	10.36	12.20			0.07	200E	60N	3		
47	10.9						297E	215S	5		
37	11.69	12.30	13.36			0.11	317E	77S	5		
36	11.62	12.13	13.44			0.11	343E	62S	5		

(a) Magnitudes given to 0.1 mag are scan magnitudes, and are uncertain by ≥ 0.3 mag. Magnitudes given to 0.01 mag are photometric magnitudes.

(b) Uncertainties are ± 1σ, and include both photometric and statistical uncertainties. The uncertainties are given only when greater than 0.05 mag for photometry; no uncertainties are given for scan magnitudes.

(c) Offset in arcsec from HD 200775 = star A.

(d) Uncertainty in arcsec of stellar position.

(e) R and RS are variable and suspected variable stars found by Rosino and Romano (1962). S are very red stars (V–[1 μm] > 3 mag) identified by Strom *et al.* (1972).

(f) Indicators used to determine which stars are probable pre-main sequence (PMS) stars. H = hydrogen line emission, I = infrared excess, V = variable.

(g) Close visual binary (Romano 1975). Photometry includes both components.

(h) T Tauri star, also known as HRC 304 and Perrine 3 in the T Tauri star catalogue of Herbig and Rao (1972).

Table 2b

Stars found in 2.2 μm scans of NGC 2023

name	K[a]	H[a]	J[a]	r[b]	$\sigma(K)$[c]	$\sigma(H)$[c]	$\sigma(J)$[c]	$\Delta\alpha$[d]	$\Delta\delta$[d]	Δpos[e]	Other designations[f]	PMS[g]
M	10.86	10.95	11.32					156W	251S	4		
J	10.70	11.10	12.01				0.06	151W	94N	4		
E	11.15	11.41	12.12	16.6			0.06	55W	115S	3		
C	8.42	9.74	11.31	16.1				30W	76S	3	S108	H,I
D	10.32	12.79	14.37			0.06	0.21	20W	105S	3		I
A	7.32	7.34	7.44					0E	0N	3	HD 37903, BD -02° 1345	
B	9.92	10.37	11.26	14.9				29E	28S	3	S101	
I	10.31	11.82	13.51				0.12	60E	51S	4		I
G	10.83	11.36	12.12	17.2			0.06	62E	125S	3		I
205				16.4				74E	126S		S106	
217				17.5				89E	44S		h	
218				17.3				90E	34S		h	
219				17.5				94E	32S		h	
F	9.26	10.74	12.47					95E	34S	3.	h	I
211				18.9				98E	81S			
220				17.6				101E	26S		h	
H	7.43	8.13	9.01					133E	65S	4	S105	H,I
K	10.12	10.99	12.91				0.07	212E	181S	4		
L	9.27	9.77	11.05					527E	39N	4		
N	8.6							667E	15N	10		

(a) K, H, and J magnitudes given to 0.1 mag are scan magnitudes, and are uncertain by $\gtrsim$ 0.3 mag. K, H, and J magnitudes given to 0.01 mag are photometric magnitudes.

(b) r magnitudes are photometric magnitudes, with typical uncertainties of 0.2 mag.

(c) Uncertainties at K, H, and J are $\pm$ 1σ, and include both photometric and statistical uncertainties. These uncertainties are given only when greater than 0.06 mag for photometry; no uncertainties are given for scan magnitudes.

(d) Offset in arcsec from HD 37903 = star A.

(e) Uncertainty in arcsec of stellar position, given only for stars measured in infrared.

(f) S = stars observed by Strom *et al.* (1975).

(g) Indicators used to determine which stars are probable pre-main sequence (PMS) stars. H = hydrogen line emission, I = infrared excess, V = variable.

(h) The region containing stars F, 217, 218, 219, 220, S102, S103, S104, and S110 is rather confused. Probably S104 = 220; S110 = 218 + 219; F = some or all of 217, 218, 219, and 220; and F = some or all of S102, S103, S104, and S110.

Table 2c

Stars found in 2.2 μm and 1.65 μm scans of NGC 2068

name	K^a	H^a	J^a	r^b	$\sigma(K)^c$	$\sigma(H)^c$	$\sigma(J)^c$	$\Delta\alpha^d$	$\Delta\delta^d$	Δpos^e	Other designations[f]	PMS[g]
1	9.0							649W	0N	10		
2	9.6							611W	29S	10	LkHα 298, SSV 51	H,I
3	10.1							406W	96N	10	SSV 54	
4		10.6						401W	344S	10	M78/111, SSV 48	I,V
5	7.98	9.06	10.46					392W	110S	10	LkHα 300, SSV 49	H,I
6	10.2							344W	181N	10		
7	11.6							326W	48S	8		
8	10.8							298W	20N	4	SSV 52	
9	11.8							286W	113N	4		
10	11.2							258W	24N	4		
11	11.1							242W	145S	4	M78-1	V
135				14.7				228W	308S			
12	11.1			16.4				218W	101N	4		
13	10.6			19.0				203W	77N	4	SSV 7	
14	10.0			16.1				177W	153S	4	M78/109, M78-2, SSV 13	V
15	11.91	12.75	13.72	18.0	0.09	0.09	0.25	173W	61N	4		I
133				17.5				163W	214N		SSV 16	
17	9.76	10.49	12.05					156W	61N	3	M78-4, SSV 6	V
16	11.2			17.5				151W	63S	8	M78-3, SSV 8	V
18	11.4							141W	226S	4		
19	9.67	11.06	13.16	16.9				133W	64N	3	M78-5, SSV 2	I,V
20	9.8	10.6		15.0				119W	242S	4	LkHα 304, M78/108, SSV 11	H,V
21	11.8			18.2				109W	81S	4		
22	12.0							105W	93N	4		
23	11.8							105W	161N	8		
24	11.1							93W	24N	4	SSV 5	
25	11.4							77W	61N	4		
26-1				20.3				69W	6S			
26a	10.15	10.48	11.51					67W	29S	3	M78/106, A	
26b	10.62	11.00	11.91					66W	18S	3	M78/107, A	
26-2				16.3				63W	17S			
26-3				15.1				61W	25S			
26-4				15.9				59W	10S			

(a) K, H, and J magnitudes given to 0.1 mag are scan magnitudes, and are uncertain by $\gtrsim$ 0.3 mag. K, H, and J magnitudes given to 0.01 mag are photometric magnitudes.

(b) r magnitudes are photometric magnitudes, with typical uncertainties of 0.2 mag.

(c) Uncertainties at K, H, and J are $\pm 1\sigma$, and include both photometric and statistical uncertainties. These uncertainties are given only when greater than 0.05 mag for photometry; no uncertainties are given for scan magnitudes.

Table 2c continued

name	K[a]	H[a]	J[a]	r[b]	σ(K)[c]	σ(H)[c]	σ(J)[c]	Δα[d]	Δδ[d]	Δpos[e]	Other designations[f]	PMS[g]
119				16.2				52W	155S			
27	12.6							35W	70N	6		
28	12.4							35W	50N	6		
29	12.3							33W	5N	3		
30	8.63	10.74	12.61	16.1			0.06	27W	274S	4	M78-10, SSV19	I
31	8.23	8.39	8.61					20W	48S	4	HD 38563-S, M78-8, i	
32	8.94	9.35	10.38	14.2				17W	6N	3	M78/104	
33	6.82	7.03	7.59					0E	0N	3	HD 38563-N, M78-9, SSV 1, i	
34	10.2			16.4				5E	10N	6		
35	11.6			16.0				5E	98S	3		
36	8.66	9.05	9.65					8E	166S	4	HD 38563-C, M78-11, SSV 9, i	
37	12.0							10E	28N	3		
38	10.6							32E	109N	3		
39	11.2							32E	218S	8		
40	10.3			16.2				41E	78S	3	M78-12	V
42	11.4			17.2				41E	3N	3		
108				18.3				42E	126S			
41	11.9			14.1				43E	49S	6		
43	11.5			20.9				44E	25S	3		
44	11.4			17.4				45E	105S	5		
45	11.4							54E	31N	3		
113				17.2				57E	61S			
46	12.0							73E	84N	8		
47	10.3	11.0		13.1				83E	41S	5	LkHα 306, M78-13, SSV 3	H,V
48	11.6							105E	93S	4		
49	11.4							117E	49N	8		
50	10.2							133E	322S	4		
51	11.4							137E	290S	4		
107				17.3				144E	157S			
52	10.9							178E	13S	4	SSV 18	
53	9.7	10.3						204E	15N	4	SSV 17	
54	11.8							240E	85S	10		
55		10.6						363E	315S	10		

(d) Offset in arcsec from HD 38563-N = star 33.

(e) Uncertainty in arcsec of stellar position, given only for stars measured in infrared.

(f) Designations beginning M78/ and M78- refer to stars found optically and by infrared searches respectively by Strom *et al.* (1975). Designations beginning SSV refer to stars found in infrared searches by Strom, Strom, and Vrba (1976).

(g) Indicators used to determine which stars are probable pre-main sequence (PMS) stars. H = hydrogen line emission, I = infrared excess, V = variable.

(h) The stars 26a and 26b together are also known as M78-6 and SSV 4.

(i) HD 38563 also known as BD +00° 1177

Table 3a

Variability in NGC 7023

Name	K^a	$\sigma(K)^b$	H^a	$\sigma(H)^b$	date^c
36	9.50				1972
36	11.0				1981JUL31
36	11.0				1981AUG01
36	11.0				1981AUG01
36	11.05		11.51		1981NOV15
J	9.2				1979AUG23
J	9.4				1979AUG24
J	9.3				1979AUG24
J	9.56		10.08		1979SEP02
J	8.97		9.62		1981JUL27
J	9.1				1981NOV20
K			10.0		1979AUG22
K	9.4				1979AUG23
K	10.2				1979AUG24
K	9.40		9.84		1979SEP02
K	9.36	0.06	9.80		1981JUL27
K	9.6				1981NOV19
E	10.50				1972
E			11.3		1979AUG22
E	10.5				1979AUG23
E	10.7				1979AUG24
E	10.60		11.13		1979SEP02
E	10.88		11.30		1981JUL26
E	11.4				1981NOV19
L			10.1		1979AUG22
L	9.4				1979AUG23
L	9.5				1979AUG23
L	9.6				1979AUG23
L	9.6				1979AUG24
L	9.55		10.05		1979SEP02
L	9.30		9.64		1981JUL27

Table 3a continued

Variability in NGC 7023

Name	K^a	$\sigma(K)^b$	H^a	$\sigma(H)^b$	date[c]
M	11.0				1979AUG23
M	11.0				1979AUG24
M	10.99		11.29		1979SEP02
M			11.42		1981JUL29
M	11.01		11.37		1981JUL30
M	11.8				1981NOV19
D	10.2				1979AUG23
D	10.04		10.30		1979SEP02
D	10.2				1979SEP03
D	10.38		10.56		1981JUL26
D	10.53		10.68		1981JUL26
D	10.3				1981NOV19
C	10.50				1972
C	9.9				1979AUG23
C	10.1				1979AUG24
C	10.1				1979AUG24
C	10.08		10.68		1979SEP02
C	10.25		10.84		1981JUL28
C	10.4				1981NOV19
T	11.19		11.49		1979SEP03
T	11.23		11.47		1981JUL29
T	11.0				1981JUL30
T	11.9				1981NOV16

(a) K and H magnitudes given to 0.1 mag are scan magnitudes, and are uncertain by $\gtrsim$ 0.3 mag. K and H magnitudes given to 0.01 mag are photometric magnitudes.

(b) Uncertainties are $\pm$ 1σ, and include both photometric and statistical uncertainties. The uncertainties are given only when greater than 0.05 mag for photometry; no uncertainties are given for scan magnitudes.

(c) Dates for which the year only is given are for observations by other observers, and refer to the year in which the data were published. The supplemental observations were taken from Strom *et al.* (1972).

Table 3b

Variability in NGC 2023

Name	K[a]	$\sigma(K)$[b]	date[c]
F	8.65	0.28	1975
F	8.5		1981JAN06
F	8.7		1981JAN06
F	9.9		1981FEB01
F	9.26		1981SEP15

(a) K magnitudes given to 0.1 mag are scan magnitudes, and are uncertain by $\gtrsim$ 0.3 mag. K magnitudes given to 0.01 mag are photometric magnitudes.

(b) Uncertainties are $\pm$ 1σ, and include both photometric and statistical uncertainties. The uncertainties are given only when greater than 0.05 mag for photometry; no uncertainties are given for scan magnitudes.

(c) Dates for which the year only is given are for observations by other observers, and refer to the year in which the data were published. The supplemental observations were taken from Strom *et al.* (1975), and are the sum of the contributions of S102, S103, S104, and S110 (see footnote to Table 2b).

Table 3c

Variability in NGC 2068

Name	K^a	$\sigma(K)^b$	H^a	$\sigma(H)^b$	date[c]
4	10.50	0.25			1975
4	9.09	0.1	10.25	0.1	1976
4			10.6		1981FEB04
11	9.8				1975
11	11.1				1981NOV20
13	10.80	0.25	11.54	0.25	1976
13	10.2				1981FEB12
13	11.0				1981NOV20
14	9.40	0.2	9.70	0.2	1975
14	9.91	0.1	10.59	0.25	1976
14	10.0				1981NOV20
15	9.3				1981FEB12
15	11.91	0.09	12.75	0.09	1981NOV19
15	12.0				1981NOV20
16	9.7				1975
16	11.07	0.25			1976
16	11.2				1981NOV18
16	11.2				1981NOV18
17	9.0				1975
17	10.08	0.1	11.04	0.25	1976
17	9.9				1981FEB06
17	9.6				1981FEB12
17	9.9				1981FEB12
17	9.8				1981NOV18
17	9.63		10.40		1981NOV19
17	9.8				1981NOV20
17	9.76		10.49		1982JAN16
19	9.2		10.3		1975
19	9.94	0.1	10.35	0.1	1976
19	9.4				1981FEB06
19	9.9				1981FEB06
19	9.0				1981FEB12
19	9.3				1981FEB12
19	10.1				1981NOV18
19	9.80		11.23		1981NOV19
19	9.67		11.06		1982JAN16

Table 3c continued

Variability in NGC 2068

Name	K^a	$\sigma(K)^b$	H^a	$\sigma(H)^b$	date[c]
20	8.90	0.2			1975
20	9.64	0.1	10.20	0.1	1976
20			10.6		1981FEB03
20	9.9				1981NOV18
20	9.7				1981NOV20
26	8.8				1975
26	9.87	0.1	10.10	0.1	1976
26			10.6		1981FEB03
26			10.3		1981FEB03
26	9.6				1981FEB12
26	9.6				1981FEB12
26	10.1				1981NOV17
26	9.74		10.15		1981NOV19
26	9.86				1981NOV19
26a	9.60	0.2			1975
26a	10.1				1981NOV18
26a	10.15		10.48		1982JAN16
26b	10.00	0.2			1975
26b	10.5				1981NOV18
26b	10.62		11.00		1982JAN16
40	9.5				1975
40	10.1				1981SEP16
40	10.1				1981NOV11
40	10.7				1981NOV17
47	9.5				1975
47	10.33	0.1	10.86	0.25	1976
47			11.0		1981FEB03
47	10.4				1981FEB12
47	9.9				1981FEB12
47	10.6				1981SEP17
47	10.2				1981SEP19
47	10.3				1981NOV17
47	10.4				1981NOV20

(a) K and H magnitudes given to 0.1 mag are scan magnitudes, and are uncertain by $\gtrsim$ 0.3 mag. K and H magnitudes given to 0.01 mag are photometric magnitudes.

(b) Uncertainties are $\pm$ 1σ, and include both photometric and statistical uncertainties. The uncertainties are given only when greater than 0.05 mag for photometry; no uncertainties are given for scan magnitudes.

(c) Dates for which the year only is given are for observations by other observers, and refer to the year in which the data were published. The supplemental observations were taken from Strom *et al.* (1975), and Strom, Strom, and Vrba (1976).

Figure Captions

Fig. 1. $J-H$ *vs.* $H-K$ colors in magnitudes of the stars observed in (*a*) NGC 7023, (*b*) NGC 2023, and (*c*) NGC 2068. Error bars are ± 1σ. Filled circles indicate observations from this paper, while open circles in Fig. 2(*c*) indicate observations from Strom, Strom, and Vrba (1976). The solid curve is the main sequence, from A0V to M5V. The solid line indicates the expected reddening line for a background K giant, while the dashed line indicates the reddening line for an A0V star.

Fig. 2. Plot of positions of stars found in (*a*) NGC 7023, (*b*) NGC 2023, and (*c*) NGC 2068. Pluses indicate stars found at 2.2 or 1.65 μm, open circles indicate stars found at 0.655 or 0.8 μm, and an asterisk indicates the visual illuminating star of each reflection nebula. The solid outline indicates the scan area for the scans at 2.2 μm from which complete samples of stars were drawn, while the dashed outline indicates additional area scanned at 2.2 μm.

Fig. 3. Cumulative counts $N(K)$ *vs.* observed K magnitude for the stars in NGC 2068. The cumulative counts are given as number of stars per square degree brighter than the observed K magnitude. Error bars are ± 1σ. The indicated line is a least squares fit of the function $N(K) = N_0\, 10^{\gamma K}$ to the data.

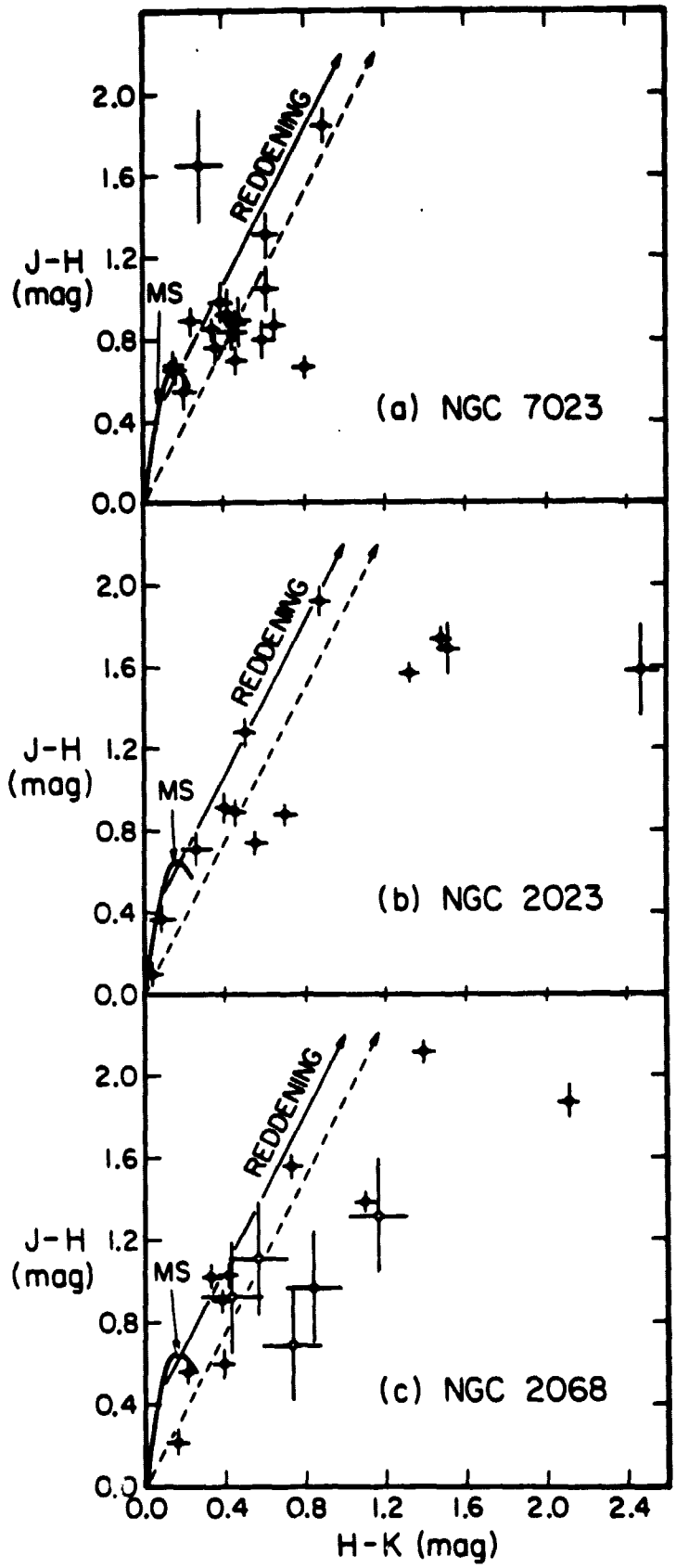
J-H (mag)
H-K (mag)
REDDENING
MS
(a) NGC 7023
(b) NGC 2023
(c) NGC 2068
0.0
0.4
0.8
1.2
1.6
2.0
2.4

Figure 1

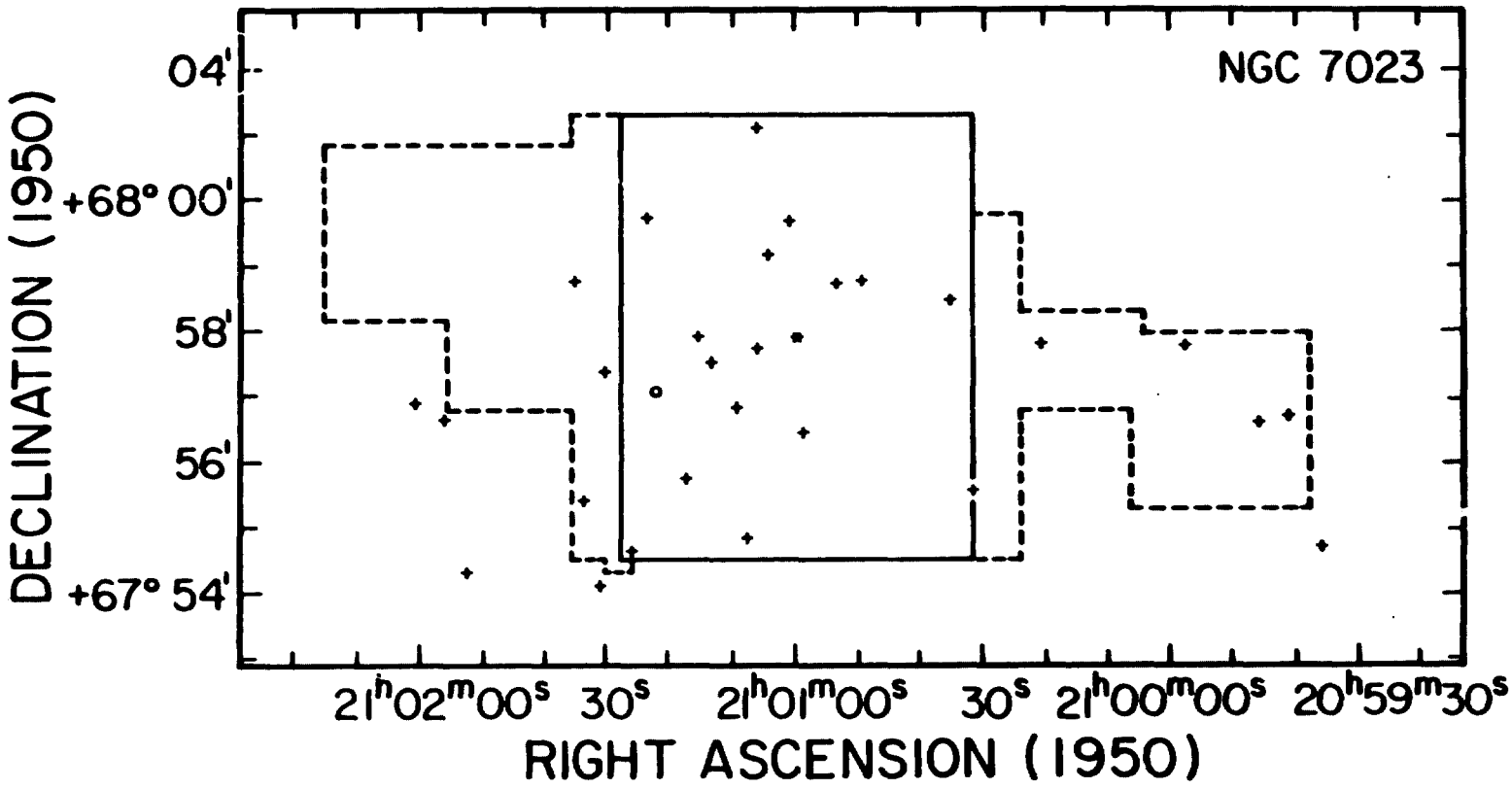
NGC 7023
04'
+68° 00'
58'
56'
+67° 54'
DECLINATION (1950)
21h02m00s
30s
21h01m00s
30s
21h00m00s
20h59m30s
RIGHT ASCENSION (1950)

Figure 2a

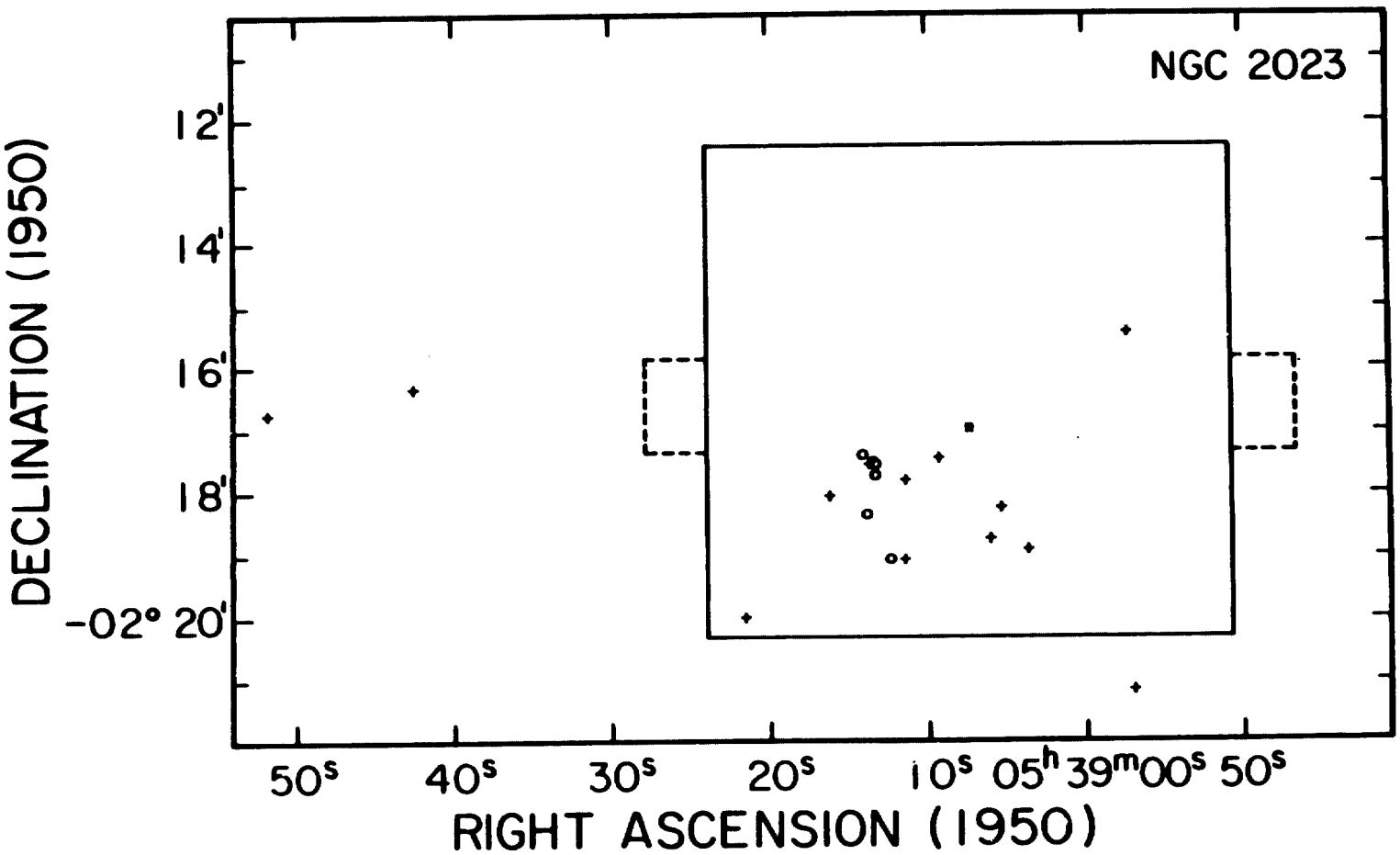
NGC 2023
DECLINATION (1950)
12'
14'
16'
18'
-02° 20'
50s
40s
30s
20s
10s
05h 39m 00s
50s
RIGHT ASCENSION (1950)

Figure 2b

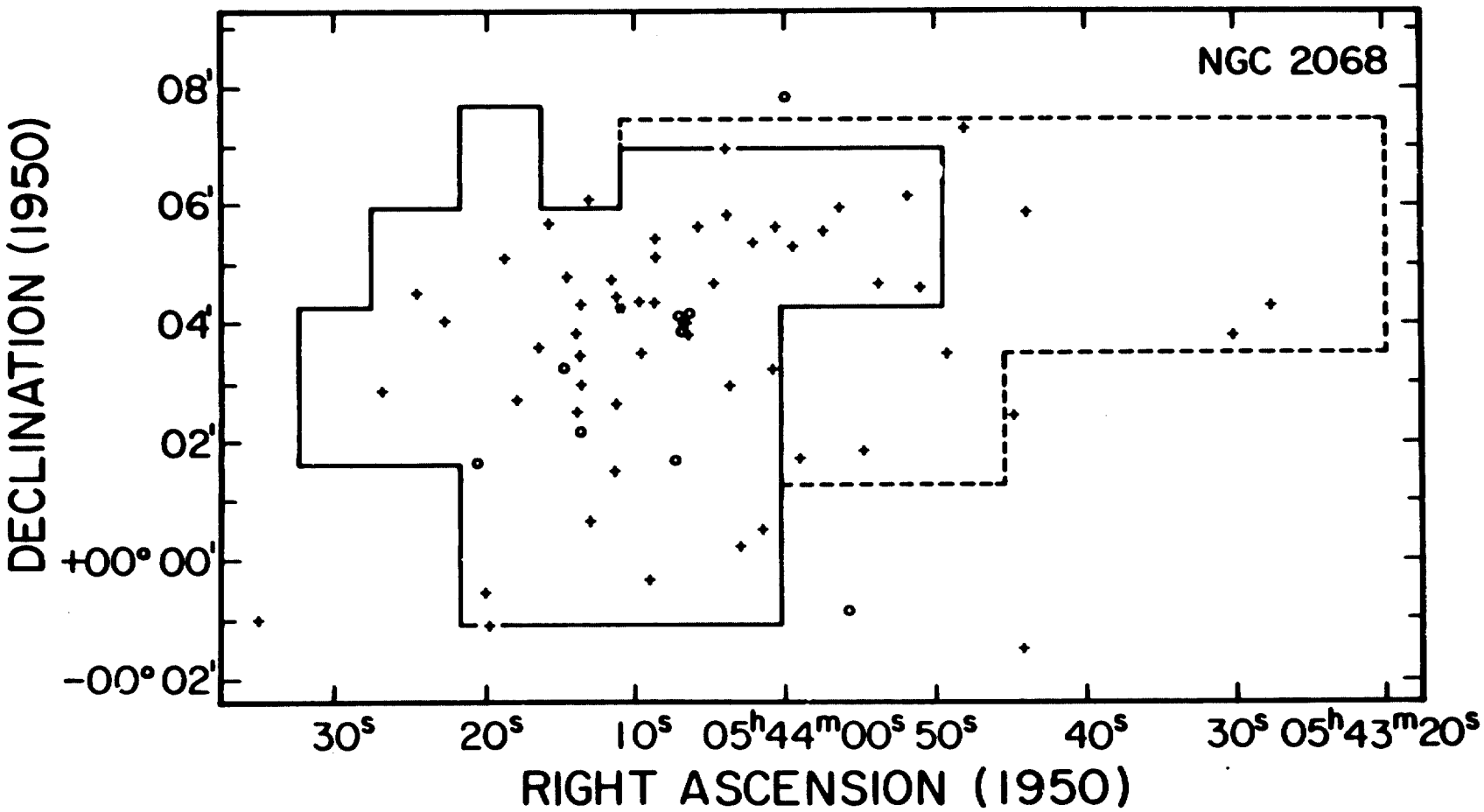
NGC 2068
08'
06'
04'
02'
+00° 00'
-00° 02'
DECLINATION (1950)
30s
20s
10s
05h44m00s
50s
40s
30s
05h43m20s
RIGHT ASCENSION (1950)

Figure 2c

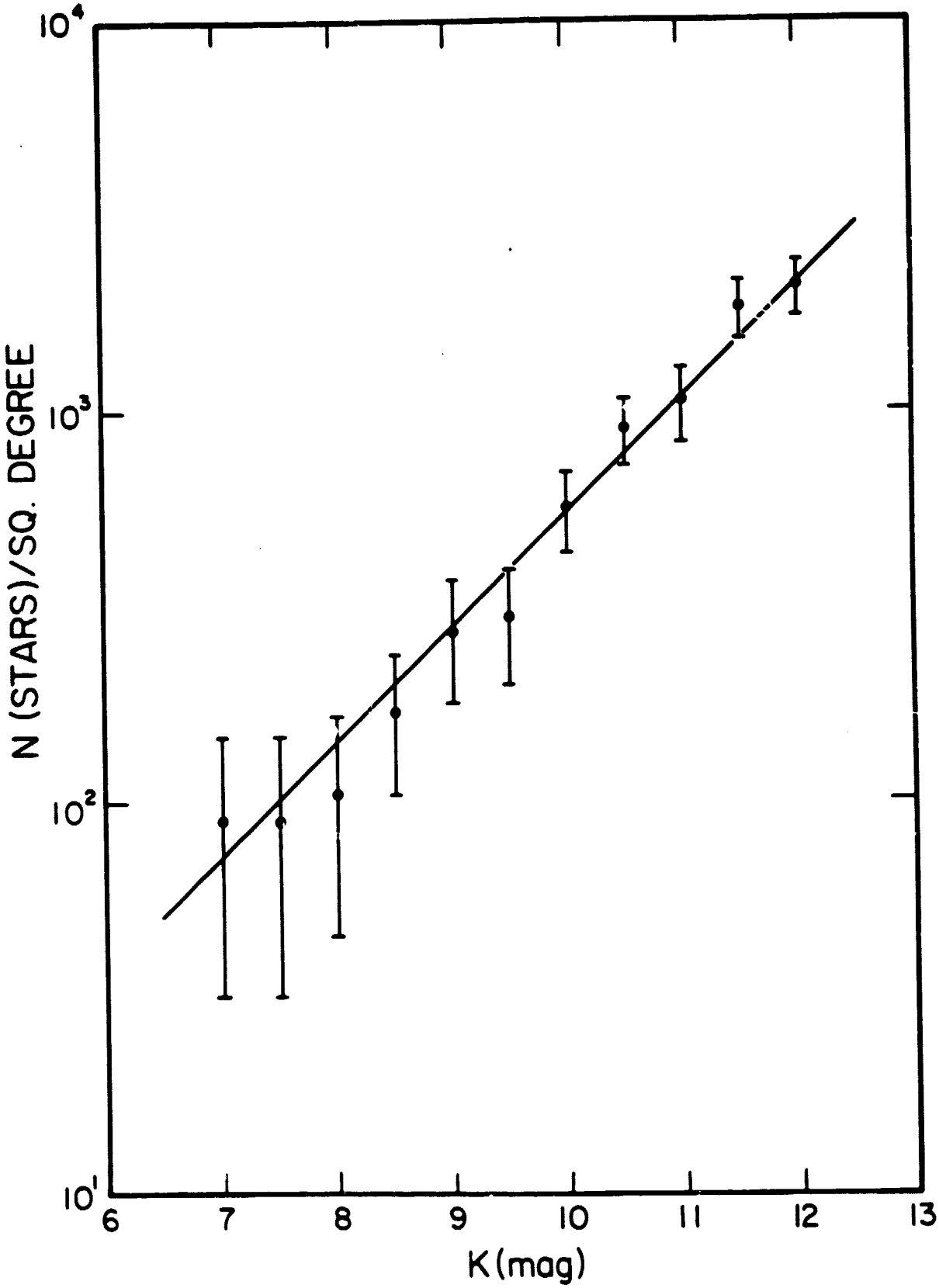

Figure 3

AUTHOR'S ADDRESS

K. SELLGREN
Physics Department
California Institute of Technology
Pasadena, CA 91125